# Phase noise mitigation in photonics-based radio frequency multiplication

MARCO SECONDINI[1,2], ANTONELLA BOGONI[1,2], ENRICO FORESTIERI[1,2], ANTONIO D'ERRICO[3], ALESSANDRA BIGONGIARI[3], AND ANTONIO MALACARNE[2,*]

[1] *TeCIP - Telecommunications, Computer Engineering, and Photonics Institute, Sant'Anna School of Advanced Studies, 56124 Pisa, Italy*
[2] *PNTLab - Photonic Networks and Technologies Nat'l Lab, CNIT - National Inter-University Consortium for Telecommunications, 56124 Pisa, Italy*
[3] *Ericsson Research, 56124 Pisa, Italy*
[*] *Corresponding author: antonio.malacarne@cnit.it*

*Compiled February 1, 2023*

**Two photonics-based radio frequency multiplication schemes for the generation of high-frequency carriers with low phase noise are proposed and experimentally demonstrated. With respect to conventional frequency multiplication schemes, the first scheme induces a selective cancellation of phase noise at periodic frequency-offset values, while the second scheme provides a uniform 3-dB mitigation of phase noise. The two schemes are experimentally demonstrated for the generation of a 110-GHz carrier by sixfold multiplication of an 18.3-GHz carrier. In both cases, the experimental results confirm the phase noise reduction predicted by theory.** 

http://dx.doi.org/10.1364/ao.XX.XXXXXX

## 1. INTRODUCTION

Current and next-generation wireless networks are mainly based on orthogonal frequency division multiplexing (OFDM) [1–4] to provide high spectral efficiency and mitigate inter-symbol interference caused by multipath fading. The radio transmission can operate at frequency carriers ranging from sub-GHz to sub-THz and use high order modulations such as 256 QAM to augment the system capacity [5]. Unfortunately, OFDM modulated signals are susceptible to phase noise (PN) [6, 7], which induces both a common phase error (CPE) and inter-carrier interference (ICI). The impact of CPE and ICI grows as the modulation order increases and the subcarrier spacing decreases [8, 9].

Simple digital processing techniques can be employed to mitigate CPE, but they are usually ineffective against ICI. The problem is particularly relevant when high-frequency carriers—typically affected by strong PN—are employed. This means that the larger bandwidth made available by using high-frequency carriers may not be exploited as OFDM carriers need a larger spacing to mitigate the effects of the increased PN.

High radio frequency (RF) carriers are commonly generated by synthesizers which produce the desired frequency by multiplying a reference frequency from a local oscillator [10]; the multiplication steps increase the inherent phase noise of the reference and may add further noise sources originated from the employed devices [11]. This results in the production of relevant phase noise in high-frequency clock signals obtained through several multiplication stages.

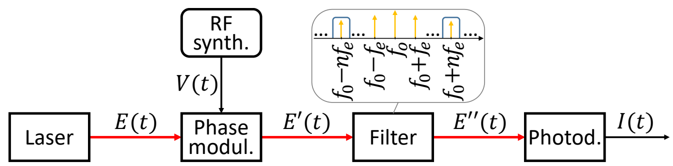


**Fig. 1.** Photonics-based radio frequency multiplication.

A convenient solution for the generation and distribution of the required high-frequency carriers is photonics-based RF generation [12] (and references therein) and, in particular, photonics-based RF multiplication [13, 14]. In this paper, two novel RF multiplication schemes to generate a high-frequency RF carrier with low PN are proposed and experimentally verified. In the first scheme, the PN of the obtained high-frequency carrier is selectively cancelled at periodic frequency offset values, with a spectral period that can be arbitrarily selected by design. RF generation up to 110 GHz with PN cancellation at odd multiples of 1 MHz frequency offset is experimentally demonstrated. The scheme can mitigate the impact of ICI in the abovementioned scenario (not demonstrated here) and is partly integrable on CMOS-compatible platform, as shown in [14], except for two spools of optical fiber that determine the frequency offset values at which PN is cancelled. In the second scheme, a uniform 3-dB mitigation of PN at all frequency offset values is obtained, through a scheme that is fully integrable as it does not require fiber delays. The PN improvement comes at the cost of using two independent clock references instead of one.

## 2. PHOTONICS-BASED RF MULTIPLICATION

A simple and versatile scheme for photonics-based RF multiplication is depicted in Fig. 1 [13]. The optical carrier generated by the laser is denoted by

$$E(t) = E_o \cos\left(\omega_o t + \phi_o(t)\right) \tag{1}$$

where $E_0$ is the amplitude, $\omega_0 = 2\pi f_o$ the angular frequency, and $\phi_o(t)$ the PN of the laser with power spectral density (PSD) $P_{\phi o}(f)$. Analogously, the electrical tone generated by the RF synthesizer is denoted by

$$V(t) = V_e \cos\left(\omega_e t + \phi_e(t)\right) \tag{2}$$

with amplitude $V_e$, angular frequency $\omega_e = 2\pi f_e$, and PN $\phi_e(t)$ with PSD $P_{\phi e}(f)$. The optical signal at the output of the phase modulator is given by

$$\begin{aligned} E'(t) &= E_o \cos\left(\omega_o t + \phi_o(t) + \beta \cos\left(\omega_e t + \phi_e(t)\right)\right) \\ &= E_o \sum_{k=-\infty}^{\infty} J_k(\beta) \cos\left((\omega_o + k\omega_e)t + \phi_o(t) + k\phi_e(t) + k\frac{\pi}{2}\right) \end{aligned} \tag{3}$$

where $\beta = \pi V_e / V_\pi$, $V_\pi$ is the half-wave voltage of the modulator, and $J_k(\beta)$ is the Bessel function of the first kind of order $k$ [13, 15]. The optical filter then selects only the $n$-th order optical sidebands, corresponding to the terms with $k = \pm n$ centered at frequencies $f = f_o \pm n f_e$, as shown in the inset in Fig. 1, obtaining

$$\begin{aligned} E''(t) &= E_o J_n(\beta) \cos\left((\omega_o + n\omega_e)t + \phi_o(t) + n\phi_e(t) + n\frac{\pi}{2}\right) \\ &+ E_o J_n(\beta) \cos\left((\omega_o - n\omega_e)t + \phi_o(t) - n\phi_e(t) + n\frac{\pi}{2}\right) \end{aligned} \tag{4}$$

Eventually, denoting by $R$ the photodetector responsivity and neglecting the DC term (irrelevant and typically removed by a DC block), the beating at the photodetector of the two terms in (4) produces the RF tone

$$I(t) = R E_o^2 J_n^2(\beta) \cos\left[2n\omega_e t + 2n\phi_e(t)\right] \tag{5}$$

whose frequency and phase equal the frequency and phase differences of the terms in (4). In practice, the frequency-multiplied RF tone (5) has $2n$ times the frequency of the original tone generated by the synthesizer, $2n$ times its PN (the two electrical PN terms are coherently added), whereas it is not affected by the optical PN (the two optical PN terms cancel out). The PSD of the PN of the frequency-multiplied RF tone is therefore

$$P_\phi(f) = (2n)^2 P_{\phi e}(f) \tag{6}$$

i.e., $(2n)^2$ times the PSD of the electrical PN.

From (4), it appears that inducing a relative delay between the two electrical PN terms would be beneficial, as it would partially decorrelate them and avoid their coherent combination; on the other hand, inducing a delay between the optical PN components would be detrimental, as it would prevent their exact cancellation. Therefore, we propose the alternative scheme in Fig. 2, where the optical carrier is split and separately processed in two branches by using two modulators, two filters, and two optical delay lines. The different order in which the modulator and the delay line are arranged in the lower and upper branches ensures that a relative delay $\tau$ is induced only between the corresponding electrical PN terms, while the optical PN terms are kept synchronized (but for a possible delay error $\Delta\tau$), obtaining

$$E_1(t) = \frac{E_o}{\sqrt{2}} J_n(\beta) \cos\left((\omega_o + n\omega_e)t + \phi_o(t - \tau - \Delta\tau) + n\phi_e(t)\right) \tag{7}$$

$$E_2(t) = \frac{E_o}{\sqrt{2}} J_n(\beta) \cos\left((\omega_o - n\omega_e)t + \phi_o(t - \tau) - n\phi_e(t - \tau)\right) \tag{8}$$

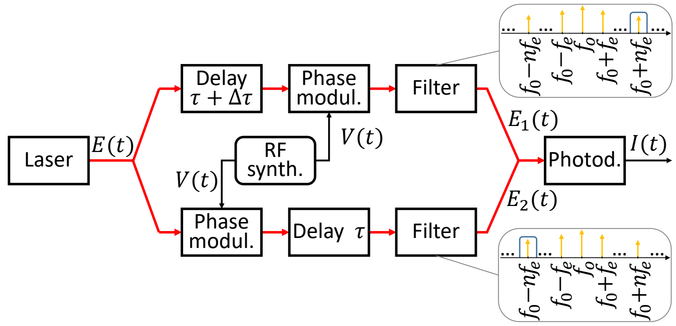


**Fig. 2.** Photonics-based radio frequency multiplication with frequency-selective PN mitigation.

where we have omitted some constant (hence irrelevant to this analysis) phase terms. The two optical signals (7) and (8) are finally recombined and photodetected. Their beating at the photodetector produces the RF tone

$$I(t) = R \left(\frac{E_o}{\sqrt{2}} J_n(\beta)\right)^2 \cos\left[2n\omega_e t + \phi(t)\right] \tag{9}$$

where we have defined the overall PN term

$$\phi(t) = n\left(\phi_e(t) + \phi_e(t - \tau)\right) + \phi_o(t - \tau - \Delta\tau) - \phi_o(t - \tau) \tag{10}$$

with PSD

$$P_\phi(f) = (2n)^2 \cos^2(\pi f \tau) P_{\phi e}(f) + 4 \sin^2(\pi f \Delta\tau) P_{\phi o}(f) \tag{11}$$

With respect to the PSD (6), obtained with the conventional scheme of Fig. 1, the impact of the electrical PN in (11) is mitigated by the $\cos^2$ term, which periodically vanishes at frequencies $f = (m + 1/2)/\tau$, with $m$ integer. On the other hand, the presence of a possible delay error $\Delta\tau$ prevents the full cancellation of the optical PN, whose contribution shows up at high frequency. It is therefore possible to select the frequency values at which the PN is cancelled by properly setting $\tau$. At the same time, it is important to make the delay error $\Delta\tau$ small enough to keep the contribution of the optical PN negligible, e.g., by making sure that the $\sin^2$ term remains small up to the frequency where $P_{\phi o}(f)$ becomes also sufficiently small. The impact of a residual delay error $\Delta\tau$ is experimentally investigated in [16].

The scheme of Fig. 2 is characterized by the presence of long optical delay lines, which might be a critical issue in the realization of a photonic integrated circuit. The scheme can be alternatively implemented with bulk devices, in which case the optical delay lines are simply realized with optical fibers. In this case, thermal and mechanical instabilities may induce a time-varying phase shift between the two optical components in (7) and (8), causing an additional PN term to appear in (10). The contribution of this additional term is limited to the low-frequency part of the PSD (typically up to a few kHz) and is usually negligible in most applications.

An alternative scheme, which avoids the use of long optical delay lines and can be more easily integrated, is shown in Fig. 3. The idea is to fully decorrelate the electrical PN terms by using two independent RF synthesizers, rather than partially decorrelate them by using a delay line as in Fig. 2. As a result, a uniform PN mitigation is obtained at all frequencies, rather than a selective PN cancellation at certain frequencies. The driving signals generated by the two RF synthesizers are

$$V_1(t) = V_e \cos\left(\omega_e t + \phi_{e1}(t)\right) \tag{12}$$

$$V_2(t) = V_e \cos\left(\omega_e t + \phi_{e2}(t)\right) \tag{13}$$

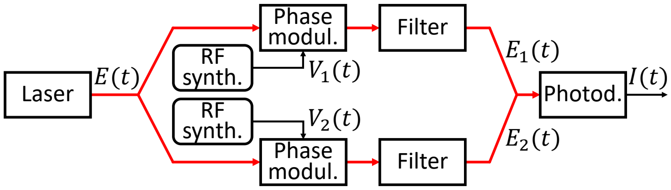


**Fig. 3.** Photonics-based radio frequency multiplication with uniform PN mitigation.

with same amplitude and frequency and affected by two independent PN realizations $\phi_{e1}(t)$ and $\phi_{e2}(t)$, respectively characterized by PSD $P_{\phi e1}(f)$ and $P_{\phi e2}(f)$. The resulting optical signals $E_1(t)$ and $E_2(t)$ can still be expressed as in (7) and (8), but with the two different electrical PNs and no relative delay ($\tau = 0$). The corresponding output photocurrent $I(t)$ is still given by (9), but with an overall PN

$$\phi(t) = n\left(\phi_{e1}(t) + \phi_{e2}(t)\right) \tag{14}$$

with PSD

$$P_{\phi}(f) = n^2\left(P_{\phi e1}(f) + P_{\phi e2}(f)\right) \tag{15}$$

For instance, assuming that $P_{\phi e1}(f) = P_{\phi e2}(f) = P_{\phi e}(f)$ (two RF synthesizers with same characteristics in terms of PN), we have $P_{\phi}(f) = 2n^2 P_{\phi e}(f)$, that is 3 dB lower than (6) at any frequency.

## 3. EXPERIMENTAL RESULTS

First, W-band carrier generation with frequency-selective PN cancellation based on the scheme depicted in Fig. 2 is experimentally demonstrated. In particular, 109.8 GHz carrier generation is targeted from sixfold multiplication ($n = 3$) of an 18.3 GHz reference clock, with noise cancellation at odd multiples of 1 MHz frequency offset. The output of an external cavity laser, with emission wavelength of 1549 nm, output power of 13 dBm and typical linewidth $\leq$ 100 kHz, is split into two branches through a fiber-based optical splitter. In the lower branch, a lithium niobate ($LiNbO_3$) phase modulator is driven by the output of an electrical synthesizer employed as the reference clock, set at a frequency of 18.3 GHz, after RF amplification up to a 27 dBm power level. Both the splitter and the modulator have polarization-maintaining single-mode-fiber (PM-SMF) pigtails. The modulator is then followed by a 100-m-long PM-SMF spool corresponding to a delay $\tau = 500$ ns. In the upper branch, another PM-SMF-pigtailed $LiNbO_3$ phase modulator, driven in the same way, is preceded by a spool of PM-SMF of equal length. Each phase modulator acts as an optical frequency comb (OFC) generator with a free spectral range (FSR) equal to the driving reference clock frequency [17]. One optical spectral line out of the generated OFC at each phase modulator output is then selected by a liquid-crystal on silicon (LCoS) WaveShaper (WS), acting as a programmable optical filter. This way, a suppression of adjacent lines no lower than 48 dB is guaranteed. The two WSs outputs are then combined through an SMF-pigtailed optical coupler. The RF tone resulting from the beating of the two selected optical modes is finally obtained at the output of a high-speed photodiode (PD) with a 3-dB bandwidth of 100 GHz. The PN PSD of the generated RF carrier is then measured with a signal source analyzer (SSA, Agilent E5052A). A microwave downconverter (E5053A) and additional external harmonic mixers are used to extend the bandwidth limitation of the instrument up to 110 GHz. Fig. 4(a) shows the optical spectra of the generated OFC (blue) and of the sideband selected by the WS (red) on the

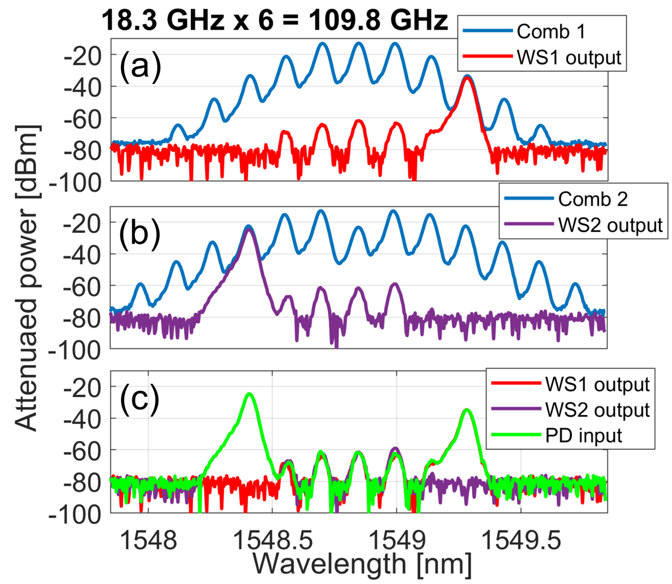


**Fig. 4.** Optical spectra: (a) upper branch, before and after the WS; (b) lower branch, before and after the WS; (c) after recombination and on each branch before recombination.

upper branch, for sixfold frequency multiplication ($n = 3$). The WS has an attenuation control range of more than 40 dB, guaranteeing that the selected sideband is at least 27 dB higher than the unselected ones. Fig. 4(b) shows the corresponding spectra (blue and purple) on the lower branch. In this case the minimum rejection of the unwanted sidebands is 34 dB. Finally, Fig. 4(c) shows the spectrum before the PD (green), after recombination of the two branches.

The measured PN PSDs shown in Fig. 5 confirm the theoretical analysis of Section 2. The blue curve is obtained by connecting a single branch of the scheme, with the WS selecting both the 110-GHz-spaced optical sidebands, as in Fig. 1. On the other hand, the yellow curve is obtained by employing the complete scheme with $\tau = 500$ ns. Finally, the red thin curve is the theoretical PSD predicted for the complete scheme, obtained by replacing $(2n)^2 P_{\phi e}(f)$ in (11) with the experimentally measured single-branch PSD. According to the theoretical prediction, the PSD obtained with the complete scheme generally follows the single-branch PSD, but is strongly attenuated at frequency offsets equal to about 1 MHz, 3 MHz, 5 MHz etc. The experimental results are in good agreement with theory, except for the frequency range $f \leq 10$ kHz, where the additional low-frequency PN caused by thermal and mechanical instabilities in the two branches of the scheme shows up, as discussed in Section 2. To partly mitigate such low-frequency noise contribution, special packaging may be used for mechanical/thermal isolation, based on double-winding fiber spool, immersion in fluids, etc. Moreover, the limited sensitivity of the measurement, due to the limited available signal power at the SSA input, makes the PN cancellation at high frequency less noticeable. Indeed, to compensate for the high loss introduced by the external harmonic mixers required to down-convert the signal before PN analysis at the SSA, optical amplification is included before the PD and the resulting optical signal-to-noise ratio ultimately determines such sensitivity level.

As a last experimental demonstration, the scheme depicted in Fig. 3 has been implemented. Two independent electrical

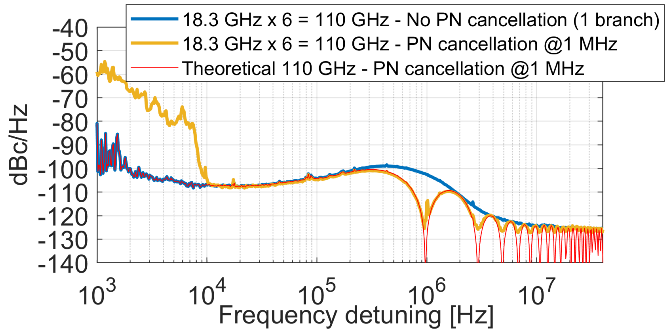


**Fig. 5.** PSD of the phase noise of the 110 GHz carrier generated with the scheme of Fig. 2.

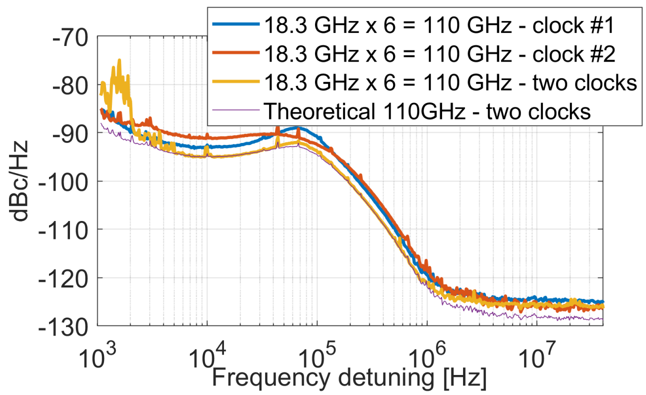


**Fig. 6.** PSD of the phase noise of the 110 GHz carrier generated with the scheme of Fig. 3.

synthesizers, clock #1 and clock #2, with PN PSD as similar as possible to each other, are now employed in the upper and lower branch, respectively. Each synthesizer drives one of the two PMs with a frequency tone at 18.3 GHz, after proper RF amplification. The two WSs select the third upper and lower sidebands of the OFC required for sixfold frequency multiplication ($n = 3$). Fig. 6 reports the measured PN PSDs of the generated RF tones at 110 GHz when only the upper branch of the setup is connected (blue), when only the lower branch is connected (red), and when both are connected and recombined before the PD (yellow). In the former two cases, the active WS selects both the upper and lower sidebands, reproducing the scheme of Fig. 1. Finally, the thin violet curve in Fig. 6 represents the theoretical PSD calculated from (15) and based on the experimentally measured PN PSDs of each clock signal. As expected, the PSD obtained with the two clocks and the full scheme of Fig. 3 is lower than the PSDs obtained with each clock and the scheme in Fig. 1. In particular, the measured PSD follows the PSD theoretically predicted by (15), except for the low-frequency range $f \leq 5\,\mathrm{kHz}$, where thermal and mechanical instabilities induce an additional low-frequency PN, and for extremely low PSD values ($\leq 120\,\mathrm{dBc/Hz}$), which are close to the sensitivity limit of the measure. Compared to the scheme of Fig. 2 and the results of Fig. 5, the low-frequency PN is significantly reduced due to the absence of the long fiber spools used as delay lines, and could be completely avoided by integrating the scheme.

## 4. CONCLUSION

Two novel schemes for PN mitigation in photonics-based RF multiplication have been proposed and experimentally demonstrated. The first scheme uses two optical delay lines to cancel PN selectively at periodic frequency-offset values, with a period that can be tailored to the specific application. However, such a solution cannot be integrated in CMOS-compatible platforms as it makes use of optical fiber-based delays. The second scheme, even though it requires two independent RF synthesizers to obtain a uniform 3-dB PN mitigation compared to a conventional scheme with a single synthesizer, is fully integrable in a CMOS-compatible platform. Both schemes have been experimentally implemented to generate a 110-GHz carrier by sixfold multiplication of an 18.3-GHz carrier. In the first scheme, the delays are selected to obtain a selective PN cancellation at odd multiples of 1 MHz frequency-offset values. The experimental results are in good agreement with the theoretical analysis and confirm the PN mitigation properties of the proposed schemes.

## ACKNOWLEDGMENTS

Portions of this work (the scheme in Fig. 2 and the experimental results in Fig. 5) were presented at the ECOC 2022 [16].

## DISCLOSURES

The authors declare no conflicts of interest.

## REFERENCES

1. 3GPP, "3GPP LTE," Releases 8-13, https://www.3gpp.org/release-8 (accessed on 22 July 2022).
2. 3GPP, "3GPP NR," Releases 14-17, https://www.3gpp.org/release-14 (accessed on 22 July 2022).
3. "Wlan," IEEE Standard 802.11, https://www.ieee802.org/11/ (accessed on 22 July 2022).
4. "Wimax," IEEE Standard 802.16, https://www.ieee802.org/16/ (accessed on 22 July 2022).
5. A. Osseiran, J. F. Monserrat, and P. Marsch, *5G mobile and wireless communications technology* (Cambridge University Press, 2016).
6. A. G. Armada and M. Calvo, IEEE Commun. Lett. **2**, 11 (1998).
7. A. G. Armada, IEEE Transactions on Broadcast. **47**, 153 (2001).
8. P. Robertson and S. Kaiser, "Analysis of the effects of phase-noise in orthogonal frequency division multiplex (OFDM) systems," in *Proceedings IEEE International Conference on Communications ICC'95*, , vol. 3 (IEEE, 1995), pp. 1652–1657.
9. A. Leshem and M. Yemini, IEEE Transactions on Signal Process. **65**, 5675 (2017).
10. J. Chen, D. Kuylenstierna, S. E. Gunnarsson, Z. S. He, T. Eriksson, T. Swahn, and H. Zirath, IEEE Transactions on Microw. Theory Tech. **66**, 3349 (2018).
11. D. B. Leeson, Proc. IEEE **54**, 329 (1996).
12. "2020 IPSR-I Integrated Photonic Systems Roadmap," https://photonicsmanufacturing.org/sites/default/files/documents/rfphotonics_ipsr-i_2020.pdf (accessed on 9 January 2023).
13. G. Qi, J. Yao, J. Seregelyi, S. Paquet, C. Bélisle, X. Zhang, K. Wu, and R. Kashyap, J. lightwave technology **24**, 4861 (2006).
14. A. Malacarne, A. Bigongiari, A. D'Errico, A. Bogoni, and C. Porzi, J. Light. Technol. (2022). Doi: 10.1109/JLT.2022.3194361.
15. M. Abramowitz and I. A. Stegun, *Handbook of mathematical functions with formulas, graphs, and mathematical tables*, vol. 55 (US Government printing office, 1972).
16. A. Malacarne, A. D'Errico, A. Bigongiari, A. Bogoni, and M. Secondini, "Frequency-selective phase noise cancellation in photonics-based radio frequency multiplication up to W-band," in *Proc. European Conference on Optical Communication*, (2022), p. We1F.3.
17. V. Torres-Company and A. M. Weiner, Laser & Photonics Rev. **8**, 368– (2014).

## FULL REFERENCES


1. 3GPP, "3GPP LTE," Releases 8-13, https://www.3gpp.org/release-8 (accessed on 22 July 2022).
2. 3GPP, "3GPP NR," Releases 14-17, https://www.3gpp.org/release-14 (accessed on 22 July 2022).
3. "Wlan," IEEE Standard 802.11, https://www.ieee802.org/11/ (accessed on 22 July 2022).
4. "Wimax," IEEE Standard 802.16, https://www.ieee802.org/16/ (accessed on 22 July 2022).
5. A. Osseiran, J. F. Monserrat, and P. Marsch, *5G mobile and wireless communications technology* (Cambridge University Press, 2016).
6. A. G. Armada and M. Calvo, "Phase noise and sub-carrier spacing effects on the performance of an OFDM communication system," IEEE Commun. Lett. **2**, 11–13 (1998).
7. A. G. Armada, "Understanding the effects of phase noise in orthogonal frequency division multiplexing (OFDM)," IEEE Transactions on Broadcast. **47**, 153–159 (2001).
8. P. Robertson and S. Kaiser, "Analysis of the effects of phase-noise in orthogonal frequency division multiplex (OFDM) systems," in *Proceedings IEEE International Conference on Communications ICC'95,* vol. 3 (IEEE, 1995), pp. 1652–1657.
9. A. Leshem and M. Yemini, "Phase noise compensation for OFDM systems," IEEE Transactions on Signal Process. **65**, 5675–5686 (2017).
10. J. Chen, D. Kuylenstierna, S. E. Gunnarsson, Z. S. He, T. Eriksson, T. Swahn, and H. Zirath, "Influence of white LO noise on wideband communication," IEEE Transactions on Microw. Theory Tech. **66**, 3349–3359 (2018).
11. D. B. Leeson, "A simple model of feedback oscillator noise spectrum," Proc. IEEE **54**, 329–330 (1996).
12. "2020 IPSR-I Integrated Photonic Systems Roadmap," https://photonicsmanufacturing.org/sites/default/files/documents/rfphotonics_ipsr-i_2020.pdf (accessed on 9 January 2023).
13. G. Qi, J. Yao, J. Seregelyi, S. Paquet, C. Bélisle, X. Zhang, K. Wu, and R. Kashyap, "Phase-noise analysis of optically generated millimeter-wave signals with external optical modulation techniques," J. lightwave technology **24**, 4861–4875 (2006).
14. A. Malacarne, A. Bigongiari, A. D'Errico, A. Bogoni, and C. Porzi, "Reconfigurable low phase noise RF carrier generation up to W-band in silicon photonics technology," J. Light. Technol. (2022). Doi: 10.1109/JLT.2022.3194361.
15. M. Abramowitz and I. A. Stegun, *Handbook of mathematical functions with formulas, graphs, and mathematical tables*, vol. 55 (US Government printing office, 1972).
16. A. Malacarne, A. D'Errico, A. Bigongiari, A. Bogoni, and M. Secondini, "Frequency-selective phase noise cancellation in photonics-based radio frequency multiplication up to W-band," in *Proc. European Conference on Optical Communication,* (2022), p. We1F.3.
17. V. Torres-Company and A. M. Weiner, "Optical frequency comb technology for ultra-broadband radio-frequency photonics," Laser & Photonics Rev. **8**, 368—-393 (2014).